

**Synthesis of highly efficient flame retardant polypropylene  
nanocomposites with surfactant intercalated  
layered double hydroxides**

Lei Qiu<sup>1, 2</sup>, Yanshan Gao<sup>1, 2\*</sup>, Cheng Zhang<sup>1, 2</sup>, Qinghua Yan<sup>1, 2</sup>, Dermot O'Hare<sup>3</sup>,

Qiang Wang<sup>1, 2\*</sup>

<sup>1</sup> College of Environmental Science and Engineering, Beijing Forestry University, 35  
Qinghua East Road, Haidian District, Beijing 100083, P. R. China

<sup>2</sup> Beijing Key Lab for Source Control Technology of Water Pollution, College of  
Environmental Science and Engineering, Beijing Forestry University, Beijing 100083,  
P. R. China

<sup>3</sup> Chemistry Research Laboratory, Department of Chemistry, University of Oxford,  
Mansfield Road, Oxford, OX1 3TA, UK

\*Corresponding author:

Yanshan Gao:

College of Environmental Science and Engineering, Beijing Forestry University, 35  
Qinghua East Road, Haidian District, Beijing 100083, P. R. China

Tel.: 86-15801531118

E-mail: yanshan\_gao@bjfu.edu.cn

Qiang Wang:

College of Environmental Science and Engineering, Beijing Forestry University, 35

Qinghua East Road, Haidian District, Beijing 100083, P. R. China

Tel.: 86-13699130626

E-mail: qiangwang@bjfu.edu.cn; qiang.wang.ox@gmail.com

## **Abstract**

The thermal and flame retardant performances of polypropylene (PP) nanocomposites with sodium dodecyl sulfate (DDS) and stearic intercalated layered double hydroxides (DDS-LDHs and stearic-LDHs) were investigated in this study. The DDS- and stearic-LDHs were treated using the aqueous miscible organic solvent treatment (AMOST) method to give highly dispersed platelets in PP composites. Incorporation of AMO-DDS- and stearic-LDH improved the thermal stability and flame retardancy of PP matrix significantly. The  $T_{0.5}$  (temperature at 50% weight loss) of PP/AMO-stearic-LDH (20 wt%) nanocomposites was dramatically increased by 80 °C compared to that of neat PP. The flame retardant performance was dependent on both surfactants and the loading of LDHs. The AMO-stearic-LDHs showed better flame retardant properties than the AMO-DDS-LDHs, especially when the LDH loading was higher than ca. 7 wt%. In addition, the stearic-LDHs with different solvothermal time including 5, 10, 24 and 72 h was studied as well. It was found out that the nanocomposites with LDHs treated by 10 h showed a best thermal stability. The PP/stearic-LDHs (24 h) nanocomposites with 20 wt% LDH loading possessed better flame retardant performance, which PHRR reduction reached to 70%.

## **Keywords**

Polypropylene; layered double hydroxides; surfactant modified; thermal stability; flame retardancy

## 1 Introduction

Layered double hydroxides (LDHs) have been shown to offer good properties in many fields like CO<sub>2</sub> adsorbent,<sup>1, 2</sup> catalyst,<sup>3, 4</sup> polymer/LDH nanocomposites<sup>5, 6</sup> and so on. Especially, LDHs could offer good flame retardancy and smoke suppression properties due to their typical chemical composition and layered structure within polymer matrix.<sup>7-9</sup> LDHs will lose their interlayer water and intercalated anions when subjected to high temperature or flame, then dehydroxylate and become a mixed metal oxide while burning. In these processes, huge amounts of heat would be adsorbed, the water released and the produced gas would also dilute the concentration of oxygen or air, which promote the formation of an expanded carbonaceous coating or char on the polymer surface, protecting the bulk polymer from being exposed to air, and suppress the production of smoke.<sup>10-12</sup> Therefore, LDHs are regarded as promising new type of environmentally friendly flame retardant additives for polymers.

In our previous studies, we synthesized Mg<sub>3</sub>Al–CO<sub>3</sub> LDHs with different morphologies including spherical, plate-like and flower-like, investigated their influence on the thermal stability and the flame retardant properties of polypropylene (PP) nanocomposites.<sup>13</sup> The results showed that the thermal stability and flame retardant properties of the nanocomposites were greatly improved after incorporating different morphologies of LDHs particles, especially with the plate-like ones. The peak heat release rate (PHRR) reduction reached to 60.7% when the LDHs loading was 29 wt%. Further, we found that different LDHs particle sizes can affect the flame retardant and mechanical properties of PP matrix as well, smaller particle sizes led to

better flame retardancy and mechanical properties.

Recently, the related experiments and their achievements of LDHs intercalated with surfactants are displayed in the people's field of vision, there are some relevant researches had been carried out. For instance, LDHs functionalized with sodium dodecylsulfonate (SDS) proved to have widely potential applications for development of new biosensors and biocatalysis.<sup>14</sup> In addition, LDH modified by the incorporation of various anionic surfactants can improve the compatibility with hydrophobic PP. According to the thermogravimetric analysis, the thermal stability of PP/organo-LDH nanocomposites was improved by 37–60 °C compared to pristine PP.<sup>15</sup> Cardanol-based surfactant modified LDHs with different loadings as flame retardant for epoxy (EP) resin had been studied as well, with only 6 wt % modified LDH (m-LDH), the composite reached a limiting oxygen index (LOI) of 29.2% and UL-94 V-0 rating, the PHRR, total heat release (THR), and total smoke production (TSP) values of EP/m-LDH-6 wt% nanocomposites were decreased by 62, 19, and 45%, respectively, compared to those of neat EP.<sup>16</sup> Kaul et al.<sup>17</sup> synthesized dodecyl sulphate (DDS) intercalated MgAl LDHs, the melamine salt of pentaerythritol diphosphate (MPP) were used as additives for the preparation of EP nanocomposites. The MgAl-DDS LDH additions to the MPP in the EP resin could protect the polymer from thermal oxidation; enhance the thermal and flammable properties of the nanocomposites. Besides, phosphorylated cellulose was used as a bio-based anion surfactant to modify LDHs (PC-LDHs), the thermal stability of polyvinyl alcohol (PVA) composites was improved after the addition of PC-LDH, and the flame

retardancy of PVA composites were significantly improved with the combination of PC-LDH as well, both PHRR and THR were reduced, the tensile strength of PVA was simultaneously improved by the increase of the LDH loading.<sup>18</sup> Till now, many studies have proved that the surfactant-LDHs within polymers can receive good properties compared to neat polymers.

In this paper, we synthesized Mg<sub>3</sub>Al LDHs with two different surfactants including sodium dodecyl sulfate (DDS) and stearic using the aqueous miscible organic solvent treatment (AMOST) method.<sup>19-25</sup> Then the PP/AMO-LDH nanocomposites were prepared using a solvent mixing method for the sake of improving the agglomeration of LDH nanoparticles in PP matrix.<sup>5</sup> The influence of AMO-DDS- and stearic-LDHs as well as different solvothermal time on the thermal stability and flame retardant properties of PP were investigated systematically.

## 2 Experimental

### 2.1 Synthesis of LDHs and PP/LDH nanocomposites

The required AMO-Mg<sub>3</sub>Al-DDS LDHs was prepared using co-precipitation method with a constant pH of 9. Generally, a 60 ml solution containing 0.027 mol Mg (NO<sub>3</sub>)<sub>2</sub>·6H<sub>2</sub>O and 0.009 mol Al (NO<sub>3</sub>)<sub>3</sub>·9H<sub>2</sub>O was added drop-wise to another 240 ml solution containing 0.018 mol DDS, in the meantime the pH of the precipitation solution was strictly controlled at ca. 9 using NaOH solution. The resulting mixture solution was hydrothermally treated at 150 °C for 12 h. And then the obtained LDHs were washed with H<sub>2</sub>O until pH=7. Later the samples were washed with methanol for

1–2 times. (For the preparation of PP/LDH nanocomposites, the methanol washed slurries were directly used without drying.) Finally, all the obtained samples were dried at 60 °C for overnight.

The AMO–Mg<sub>3</sub>Al–stearic LDHs was prepared using the co–precipitation method as well. Briefly, a 150 ml absolute methanol solution containing 0.0375 mol Mg (NO<sub>3</sub>)<sub>2</sub>·6H<sub>2</sub>O, 0.0125 mol Al (NO<sub>3</sub>)<sub>3</sub>·9H<sub>2</sub>O and 0.026 mol stearic was treated by oil bath heating at 80 °C until the solution become clear. The pH of the solution was slowly controlled to ca. 10 using NaOH solution. The resulting mixture solution was kept stirring under oil bath heating for 12 h. Then the resulting solution was solvothermally treated at 150 °C for 10 h. The obtained LDHs were treated as the former.

PP/LDH nanocomposites were prepared using a solvent mixing method. In general, 5 g PP (with a molecular weight of ca. 300000), the methanol washed LDH slurries prepared above, and 100 ml xylene was charged into round bottom flask. The amounts of LDHs corresponding to PP were controlled to be 5, 10, 15, and 20 wt%, respectively. The mixture was refluxed at approximately 140 °C for about 2–3 h until the mixed solution became clear. After the completion of the reflux process, the hot xylene solution containing the dissolved PP and highly dispersed AMO–surfactants–LDH nanoparticles was poured into 100 ml hexane for cooling. The prepared PP/LDH nanocomposites were treated by filtration and vacuum drying successively, finally the required nanocomposite samples were obtained.

## 2.2 Characterization of LDHs and PP/LDH nanocomposites

The XRD patterns of all the samples including LDHs and nanocomposites were recorded on a Shimadzu XRD-7000 diffractometer with Cu K $\alpha$  radiation, the accelerating voltage of work was set to 40 kV with 30 mA current ( $\lambda=1.542 \text{ \AA}$ ). The diffraction patterns were obtained within the confines of 2 to 70° with a slit size of 1°, whose scanning rate is 5° min<sup>-1</sup>. SEM analysis was carried out on a JEOL JSM 6700F scanning microscope based on an acceleration voltage of 5.0 kV, the powder samples were glued on the carbon tape and attached to the metal stage. Then a thin layer of platinum was sputtered on the surface of the samples to prevent charging, while the image quality can be improved as well. TEM analysis was performed on a JEOL JEM-1010 microscope with an accelerating voltage of 80 kV, samples were dispersed in ethanol by ultrasonic treatment and then dropped onto copper TEM grids coated with a lacey carbon film.

### 2.3 Thermal stability and flame retardant properties of PP/LDH nanocomposites

The thermal stability of all the nanocomposite samples were tested and analyzed by TGA (TGAQ50, TA Instruments-Waters LLC), which was performed at a heating rate of 10 °C min<sup>-1</sup> and an air flow rate of 50 ml min<sup>-1</sup> from 25 to 600 °C. Meanwhile the flammability properties of synthesized nanocomposites as well as neat PP were evaluated by Micro-scale combustion calorimeter (Model MCC-2, Govmark Organization, Inc.). In this test, the heat release rate (HRR) in W g<sup>-1</sup> (calculated from the oxygen depletion measurements), heat release capacity (HRC) in J g<sup>-1</sup> K<sup>-1</sup> (obtained by dividing the sum of the peak HRR by the heating rate in K s<sup>-1</sup>), and the total heat release (THR) in kJ g<sup>-1</sup> (given by integrating the HRR curve) of all the



synthesized nanocomposite samples could be obtained.

### 3 Results and discussion

#### 3.1 Characterization of AMO-Mg<sub>3</sub>Al-DDS, Mg<sub>3</sub>Al-stearic LDHs and their corresponding PP/LDH nanocomposites

The above obtained AMO-Mg<sub>3</sub>Al-DDS LDHs and AMO-Mg<sub>3</sub>Al-stearic LDHs were characterized using XRD analysis firstly, as shown in Fig. 1(a). Several characteristic peaks such as (003), (006), (009), and (110) planes were observed for both LDHs, indicating that the obtained LDH samples were synthesized successfully and had a well-developed layer structure. The XRD patterns also showed that the DDS and stearic intercalated LDHs resulted in different basal spacing. The basal spacing of AMO-Mg<sub>3</sub>Al-stearic LDHs was determined to be 3.20 nm, which was larger than the AMO-Mg<sub>3</sub>Al-DDS LDHs whose basal spacing was 2.58 nm. This result can be attributed to the length difference of the carbon chain between DDS and stearic (insert images in Fig. 1(b)). At the meantime, the XRD patterns of PP and its nanocomposites with LDH loadings of 5, 10, 15, and 20 wt% are shown in Fig. 1(b-c). The characteristic peaks of LDHs such as (003), (006), and (009) was clearly seen in the nanocomposites. Moreover, the intensity of the peaks represents LDHs increased with increasing of LDH loading, suggesting that LDHs with different surfactants and different loadings were introduced into PP matrix successfully

The morphology and corresponding particle size of LDHs with different surfactants were characterized by TEM analysis. Fig. 2 shows the TEM images of

AMO-Mg<sub>3</sub>Al-DDS and AMO-Mg<sub>3</sub>Al-stearic LDHs. According to Fig. 2, both DDS and stearic intercalated LDHs had formed plate-like nanoparticles, which particle sizes were around 80–150 nm. Meanwhile the growth of LDHs was ideal, laying a well foundation for the follow-up single variable experiments of the influence of surfactants on PP/LDH nanocomposites.

The distribution of surfactants modified LDHs and the morphology of the synthesized PP/LDHs nanocomposites were characterized using SEM analysis. Fig. 3 lists the images of neat PP, as well as PP/AMO-DDS-LDH and PP/AMO-stearic-LDH nanocomposites with the LDH loading of 5 and 20 wt%, respectively. According to the SEM results, PP material has no obvious change after adding AMO-DDS-LDHs or AMO-stearic-LDHs. Also, LDHs kept unchanged morphology after being introduced into PP matrix. Both LDHs have a good dispersion within PP matrix as well the plate-like LDH nanoplatelets were regularly dispersed in PP and increased with increasing of the LDHs loading.

### 3.2 Performance test of PP/AMO-DDS-LDH and PP/AMO-stearic-LDH nanocomposites

In the previous researches, we found out that LDHs with different morphologies and sizes could affect the thermal stability and the flame retardancy of PP nanocomposites.<sup>24</sup> In this contribution, the effect of the modified LDHs on the thermal stability of PP/LDH nanocomposites was studied by TGA, as shown in Fig. 4 and Table 1. The results showed that all of the  $T_{0.5}$  (temperature at 50% weight loss) values of PP based nanocomposites were increased obviously after the incorporation

of LDH nanoparticles. For PP/AMO–DDS–LDH nanocomposites, the values of  $T_{0.5}$  were increased from 331 °C to 360, 368, 354 and 343 °C with the LDH loading of 5, 10, 15 and 20 wt%, respectively. While the  $T_{0.5}$  values of PP/AMO–stearic–LDH nanocomposites were increased to 367, 398, 406 and 411 °C with the LDH loading of 5, 10, 15 and 20 wt%, respectively. However, compared to neat PP, the  $T_{0.1}$  (temperature at 10% weight loss) values of PP/AMO–DDS–LDH nanocomposites were decreased. It is because that in the initial stage of the thermal stability test, the addition of AMO–DDS–LDHs could promote and catalyze the degradation of PP in a small extent. With the LDH loading increasing, the  $T_{0.1}$  dropped more. However, the  $T_{0.5}$  and  $T_{0.1}$  of PP/AMO–stearic–LDH nanocomposites were both improved, and  $T_{0.5}$  increased with increasing the loading successively, demonstrating that the thermal stability of AMO–stearic–LDH improved with the increasing of LDH loading within the experimental range. According to the  $T_{0.5}$  graph (Fig. 4(c)), AMO–stearic–LDHs were much better than AMO–DDS–LDHs in terms of their thermal stability for PP. The  $T_{0.5}$  value was increased by 67 °C of PP/AMO–stearic–LDH nanocomposites compared to neat PP while only increased by 37 °C for PP/AMO–DDS–LDH nanocomposites when the LDH loading was 10 wt%. What is more, it is noteworthy that the  $T_{0.5}$  of PP/AMO–DDS–LDH nanocomposites was increased with the increase of LDH loading when the loading was low, and showed a highest  $T_{0.5}$  value (368 °C) when the loading of LDHs was 10 wt%. But differently, the  $T_{0.5}$  of PP/AMO–stearic–LDH nanocomposites increased with the increasing of LDH loading in PP. And when the LDH loading was 20 wt%, the value of  $T_{0.5}$  reached to 411 °C,

which was increased by 80 °C compared to neat PP (331 °C). The reason for this dramatically improved performance is not known at this time, it may be the structure of or mass fraction of the intercalated surfactant. From the SEM images (Fig. 3) the incorporation of AMO–stearic–LDHs affects the surface texture of the PP/LDH composite,<sup>26</sup> and as a result the emission of small molecules may be restrained during the degradation of PP. (It is said that the stability of PP material manifested by the weight loss when heating would be improved.) Another factor may be the presence of basic LDHs may induce slight difference in the degradation process of PP, leading to a difference on the thermal stability.<sup>27-29</sup> The presence of stearic may alleviate the alkaline degradation of PP. However, the mechanism of the thermal degradation of PP needs to be explored further.

MCC was used to determine the basic chemical heat value of PP and its nanocomposites, which can be utilized to measure the parameters of flammability properties of PP material in a short time with a very little dosage of the samples (ca. 5 mg). The heat release rate (HRR), heat release capacity (HRC), total heat release (THR),  $T_{\max}$  and so on can be obtained by using the MCC analysis. The results could predict the fire resistance of the nanocomposites, evaluating the flame retardancy of these PP/LDH nanocomposites, and make a reasonable estimation of the fire hazard for the samples. The results of MCC analysis were listed in Fig. 5 and Table 2. The PHRR of all the nanocomposite samples were obviously decreased with the addition of LDHs. Both AMO–DDS and stearic–LDHs exhibited a good flame retardant performance for PP. When the LDHs loading was 5, 10, 15, and 20 wt%, the PHRR

reduction of PP/AMO-DDS-LDH nanocomposites was 37%, 48%, 54%, and 58%, respectively. Compared to DDS intercalated LDHs, AMO-stearic-LDHs showed a slightly better flame retardancy for PP. The PHRR value decreased by 33%, 51%, 54%, and 61%, respectively with 5, 10, 15, and 20 wt% LDHs in PP. These illustrated that LDHs intercalated with different surfactants could greatly improve the combustion performance of PP material to a certain extent, as well as reduce the heat release of PP, reaching the purpose of delayed burning. At the same time, it was found that the higher the loading of LDHs is, the lower the PHRR of nanocomposites is. With the LDH loading increased, the reduction of the PHRR of PP/AMO-stearic-LDH nanocomposites presented a trend of linear rise. Although the PHRR of PP/AMO-DDS-LDH nanocomposites were also increased, the overall magnitude of it is lower than the former's, and has a trend of being gentle (Fig. 5(c)). Generally, the flame retardant performance of PP/AMO-stearic-LDH nanocomposites was better than PP/AMO-DDS-LDH nanocomposites with the increasing of LDH loading.

THR is another significant parameter for fire hazard evaluation of nanocomposites. During the MCC test, THR begins to increase steadily after ignition, and as the burning time increase, a steady state will be reached before flameout.<sup>23</sup> Therefore, the reduction in THR can be a referential evaluation for the flame retardancy of the nanocomposites. According to Table 2, both THR values were reduced apparently with increasing of the LDH loading for two types of LDHs. Comparing to neat PP, whose THR value is  $47.4 \text{ kJ g}^{-1}$ , PP/AMO-DDS-LDH

nanocomposites showed a best THR value of  $27.0 \text{ kJ g}^{-1}$  with a LDH loading of 15 wt%, PP/AMO–stearic–LDH nanocomposites showed a best THR value of  $30.7 \text{ kJ g}^{-1}$  with a LDH loading of 20 wt%, respectively. Aimed at this parameter, the DDS one is better than the stearic one.

Necessarily, HRC is also important for the work of predicting and evaluating the fire hazard of materials. Table 2 shows the values of HRC of neat PP and its nanocomposites. After the addition of LDHs with different surfactants, this parameter was decreased for all the samples compared to neat PP, which showed a highest value of  $1170 \text{ J g}^{-1} \text{ K}^{-1}$ . For example, with 20 wt% AMO–DDS–LDHs and 15 wt% AMO–stearic–LDHs, the HRC of the nanocomposites were reduced to 717 and  $722 \text{ J g}^{-1} \text{ K}^{-1}$ , reached a lowest value, respectively. Similar to THR results, the influence on the combustion performance expressed by HRC of PP/AMO–DDS–LDH nanocomposites was better than that of PP/AMO–stearic–LDH nanocomposites. Although the values of HRC and THR of PP/AMO–DDS–LDH nanocomposites were slightly higher than PP/AMO–stearic–LDH nanocomposites, as for the PHRR of nanocomposites and its reduction compared to neat PP, the influence of PP/AMO–stearic–LDH nanocomposites was greater than PP/AMO–DDS–LDH nanocomposites. In addition, with the increasing of LDH loading, this advantage became more obvious, presenting an upward trend. Also, we noticed that the  $T_{\max}$  of PP/AMO–DDS–LDH nanocomposites decreased slightly with the increasing of LDHs loading, especially when introduced 15 wt% AMO–DDS–LDHs whose value of  $T_{\max}$  was the closest to neat PP ( $478.6 \text{ }^{\circ}\text{C}$ ). At the same time, the  $T_{\max}$  of

PP/AMO–stearic–LDH nanocomposites decreased obviously compared to neat PP, and reached to a lowest level (460.8 °C) when LDH loading was 5 wt%. Considering these relevant parameters in the flame retardant test including PHRR, THR and HRC, as well as  $T_{\max}$ , it was found out that the PP/AMO–stearic–LDH nanocomposites presented a better performance than PP/AMO–DDS–LDH nanocomposites.

### 3.3 Characterization of more kinds of AMO–stearic–LDHs and its PP/LDH nanocomposites

Considering that AMO–stearic–LDHs has better performance between the above two kinds of LDHs, we additionally synthesized three different types of AMO–stearic–LDHs by controlling the solvothermal time (5, 10, 24 and 72 h), investigating the influence of particle sizes and morphologies on the thermal stability and flame retardant of PP nanocomposites.

Firstly, XRD analyses were performed for the synthesized LDHs, as shown in Fig. 6(a). It showed that the characteristic peaks such as (003), (006), (009), and (110/113) planes were clearly observed for all the AMO–stearic–LDHs, indicating that the LDH samples with different solvothermal time were synthesized successfully. The basal spacing was 3.19, 3.20, 3.09, and 2.24 nm, respectively (solvothermal time: 5, 10, 24, and 72 h). Meanwhile the XRD reflections of the PP nanocomposites are shown in Fig. 6(b). The characteristic peaks of LDHs can be clearly indexed in the nanocomposites. For the same LDHs in PP, the intensity of the peaks increased with the increasing of LDH loading, suggesting that the AMO–stearic–LDHs were introduced into PP matrix successfully with different loadings.

The particle sizes and morphologies of the AMO–stearic–LDHs were characterized by using TEM, as shown in Fig. 7. With different solvothermal time, the AMO–stearic–LDHs grew differently. When treated under 5 h (Fig. 7(a)), LDHs began to dissolve and develop to plate–like, but the plate–like is not completely formed. So under this condition, the LDHs showed a transition state, it was a combination of plate–like and flower–like. As the time increased to 10 h, as shown in Fig. 7(b), the LDHs has been completely dissolved from a flower–like to plate–like, showing a more mature independent plate–like structure, but the profile of it is not clear, as well as the particle size is relatively smaller, which was about 80–100 nm. While the time raised to 24 h (Fig. 7(c)), the particle size of LDHs grew bigger but not very obvious, with which a particle size about 100–200 nm. The LDHs developed to mature plate–like morphology when treated for 72 h. From these TEM results it is not difficult to see that with the increasing of the solvothermal time, there is no significant effect on the particle size of the AMO–stearic–LDHs, but the LDH samples were gradually dissociated from the flower–like structure into dispersed plate–like nanosheets.

#### 3.4 Performance test of more kinds of PP/AMO–stearic–LDHs nanocomposites

The influence of AMO–stearic–LDHs with different solvothermal time on the thermal stability of the nanocomposites was studied by TGA, results as shown in Fig. 8 and Table 3. Through Fig. 8(a), the  $T_{0.5}$  of PP/AMO–stearic–LDHs (10 h) nanocomposites was higher than PP/AMO–stearic–LDHs (5 h). When the LDH loading was 20 wt%, the  $T_{0.5}$  was increased by 80 and 58 °C, respectively. The lower stability above may



resulted from the bigger thermal contact area of LDHs with the 3D flower-like structure. Fig. 8(c) presents the lateral comparison of  $T_{0.5}$  with different loading in different solvothermal time, which illustrated that  $T_{0.5}$  of all the nanocomposites increased with the increasing of LDH loading when under 20 wt%. The PP/AMO-stearic-LDH (10 h) nanocomposites showed a best thermal stability compared to others, whether the loading was 15 or 20 wt%. Although the PP/stearic-LDH (5 h) and the PP/AMO-stearic-LDH (72 h) nanocomposites have similar low thermal stability embodied by the values of  $T_{0.5}$ , the reason of this phenomenon may not identical. The lower  $T_{0.5}$  of PP/AMO-stearic-LDH (5 h) nanocomposites mainly due to its 3D flower-like structure, for which can increase the ability of thermal contact and decompose in the heating process to a certain extent, consequently it did not play a very good thermal stabilizer during the decomposition of PP. As for PP/AMO-stearic-LDH (72 h) nanocomposites, the bigger particle size of the LDHs has resistance to enter the folds of PP matrix, as well as the inhomogeneity resulted from the aggregation of nanoplates, leading to the lower thermal stability. Thus we suggest that the LDHs inserted with stearic anions should be provided with a proper temperature and appropriate treated time such as 10 h, which can lead to a better thermal stability within polymers.

Subsequently MCC was used to evaluate the flame retardancy of PP/AMO-stearic-LDH nanocomposites, as shown in Fig. 9 and Table 4. The PHRR values of all samples were decreased significantly after incorporating different AMO-stearic-LDHs. For the PP/AMO-stearic-LDHs (5, 10, 24, and 72 h)

nanocomposites with 15 wt% LDHs, the PHRR reduced by 65, 54, 70, and 52%, respectively. The nanocomposites with 24 h treated LDH showed a best flame retardancy performance. The samples which were under 10 h treatment with the best thermal stability presented a lower PHRR reduction value compared to others. This is partly related to thermal decomposition capacity, when the thermal stability is lower the composites were decomposed in a short time and formed a carbon protective layer on the surface of the nanocomposites quickly, which isolate air and inhibit further combustion of composites, improving the flame retardancy efficiently. On the contrary, the carbon protective layer would be formed slowly, which makes the flame retardancy relatively worse.

For another flame retardant evaluation parameter THR, the value of all the nanocomposite samples were reduced dramatically compared to neat PP. With 15 and 20 wt% AMO–stearic–LDHs loading, there wasn't significant difference for PP/AMO–stearic–LDH (5 h) and PP/AMO–stearic–LDH (24 h) nanocomposites, both of them reached to a lowest value. Combining the combustion performance parameters of all the PP/AMO–stearic–LDH nanocomposites, the AMO–stearic–LDHs with 24 h solvothermal time within PP matrix proved to be the best among these samples, which showed a good flame retardancy. In the meantime, HRC was also used to help predicting and evaluating the fire hazard of polymer composites. Through the HRC results, when the stearic–LDH (5 h) loading was 15 wt%, the value decreased to  $982 \text{ J g}^{-1} \text{ K}^{-1}$ , which was lower than that of neat PP ( $1180 \text{ J g}^{-1} \text{ K}^{-1}$ ). When the LDHs loading increased to 20 wt%, the value of HRC further

decreased to  $524 \text{ J g}^{-1} \text{ K}^{-1}$ . Similar result was obtained in the PP/AMO–stearic–LDHs with 24 h treatment with the loading of 15 and 20 wt%, which decreased to 995 and  $487 \text{ J g}^{-1} \text{ K}^{-1}$ , respectively. Slightly differently, when the stearic–LDHs treated with 10 h and 72 h, the HRC value slightly increased with the increasing of LDHs loading. The HRC results also showed that the stearic–LDHs under 24 h solvothermal time proved to be the better flame retardant behavior.

#### **4 Conclusions**

In this contribution, the influence of DDS and stearic intercalated  $\text{Mg}_3\text{Al}$  LDHs as well as the solvothermal reaction time of AMO– $\text{Mg}_3\text{Al}$ –stearic LDHs on the thermal stability and the flame retardancy performance of PP/LDH nanocomposites was investigated. The prepared nanocomposites presented obviously improved thermal stability and fire retardant performance compared to neat PP. The  $T_{0.5}$  of PP/AMO–stearic–LDH (20 wt%) nanocomposites was dramatically increased by  $80^\circ\text{C}$ . The flame retardant results showed that the AMO–stearic–LDHs was better than the AMO–DDS–LDHs, especially when the LDH loading was relatively high. Furthermore, the obtained results showed that the PP/AMO–stearic–LDH (under 10 h solvothermal time) nanocomposites present a best thermal stability. MCC analysis revealed that the 20 wt% AMO–stearic–LDHs loading with 24 h solvothermal time showed the best flame retardancy performance, which PHRR reduction value was nearly 70%. Therefore, we suggest that both reaction time and hydrothermal (solvothermal) condition should be taken consideration to the synthesis of

AMO–stearic–LDHs, so that lead to a better thermal stability and flame retardancy within polymers.

## Acknowledgments

This work was supported by the Fundamental Research Funds for the Central Universities (2016ZCQ03), the National Natural Science Foundation of China (51622801, 51572029), and the Beijing Excellent Young Scholar (20150000026833ZK11).

## References

1. J. Wang, X. Mei, L. Huang, Q. Zheng, Y. Qiao, K. Zang, S. Mao, R. Yang, Z. Zhang, Y. Gao, Z. Guo, Z. Huang and Q. Wang, *J. Energy Chem.*, 2015, **24**, 127-137.
2. Q. Qin, J. Wang, T. Zhou, Q. Zheng, L. Huang, Y. Zhang, P. Lu, A. Umar, B. Louis and Q. Wang, *J. Energy Chem.*, 2017, **26**, 346-353.
3. Y. Zhao, M. Wei, J. Lu, Z. L. Wang and X. Duan, *Acs Nano*, 2009, **3**, 4009-4016.
4. L. Zhou, M. Shao, M. Wei and X. Duan, *J. Energy Chem.*, 2017.
5. Q. Wang, X. Zhang, C. J. Wang, J. Zhu, Z. Guo and D. O'Hare, *J. Mater. Chem.*, 2012, **22**, 19113-19121.
6. Z. Cui and B. Qu, *Chinese J. Polym. Sci.*, 2010, **28**, 563-571.
7. L. Wang, X. He, H. Lu, J. Feng, X. Xie, S. Su and C. A. Wilkie, *Polym. Advan. Technol.*, 2011, **22**, 1131-1138.
8. F. L. And and J. P. Besse, *Chem. Mater.*, 2006, **13**, 3507-3515.

9. M. Zammarano, M. Franceschi, S. Bellayer, J. W. Gilman and S. Meriani, *Polymer*, 2005, **46**, 9314-9328.
10. D. G. Evans and X. Duan, *Chem. Commun.*, 2006, **37**, 485-496.
11. S. Xu, L. Zhang, Y. Lin, R. Li and F. Zhang, *J. Phys. Chem. Solids*, 2012, **73**, 1514-1517.
12. U. Costantino, A. Gallipoli, M. Nocchetti, G. Camino, F. Bellucci and A. Frache, *Polym. Degrad. Stabil.*, 2005, **90**, 586-590.
13. L. Qiu, Y. Gao, X. Yan, J. Guo, A. Umar, Z. Guo and Q. Wang, *RSC Adv.*, 2015, **5**, 51900-51911.
14. M. Li, S. Chen, F. Ni, Y. Wang and L. Wang, *Electrochim. Acta*, 2008, **53**, 7255-7260.
15. J. H. Yang, W. Zhang, H. Ryu, J. H. Lee, D. H. Park, J. Y. Choi, A. Vinu, A. A. Elzatahry and J. H. Choy, *J. Mater. Chem. A*, 2015, **3**, 22730-22738.
16. X. Wang, E. N. Kalali and D. Y. Wang, *ACS Sustain. Chem. Eng.*, 2015, **3**, 3281-3290.
17. P. K. Kaul, A. J. Samson, G. T. Selvan, I. V. M. V. Enoch and P. M. Selvakumar, *Appl. Clay Sci.*, 2017, **135**, 234-243.
18. W. Wang, Y. Kan, H. Pan, Y. Pan, B. Li, K. M. Liew and Y. Hu, *Compos. Part A-Appl. S.*, 2017, **94**, 170-177.
19. Q. Wang and D. O'Hare, *Chem. Commun.*, 2013, **49**, 6301-6303.
20. C. Chen, M. Yang, Q. Wang, J. C. Buffet and D. O'Hare, *J. Mater. Chem. A*, 2014, **2**, 15102-15110.

21. Q. Wang, J. P. Undrell, Y. Gao, G. Cai, J. C. Buffet, C. A. Wilkie and D. O'Hare, *Macromolecules*, 2013, **46**, 6145-6150.
22. Q. Wang, X. Zhang, J. Zhu, Z. Guo and D. O'Hare, *Chem. Commun.*, 2012, **48**, 7450-7452.
23. Y. Gao, Q. Wang, J. Wang, L. Huang, X. Yan, X. Zhang, Q. He, Z. Xing and Z. Guo, *ACS Appl. Mater. Inter.*, 2014, **6**, 5094-5104.
24. N. P. Funnell, Q. Wang, L. Connor, M. G. Tucker, D. O'Hare and A. L. Goodwin, *Nanoscale*, 2014, **6**, 8032-8036.
25. P. Lu, S. Liang, L. Qiu, Y. Gao and Q. Wang, *J. Membrane Sci.*, 2016, **504**, 196-205.
26. S. Pradhan, F. R. Costa, U. Wagenknecht, D. Jehnichen, A. K. Bhowmick and G. Heinrich, *Eur. Polym. J.*, 2008, **44**, 3122-3132.
27. L. Du, B. Qu and M. Zhang, *Polym. Degrad. Stabil.*, 2007, **92**, 497-502.
28. L. Du, B. Qu, Y. Meng and Q. Zhu, *Compos. Sci. Technol.*, 2006, **66**, 913-918.
29. S. Guo, C. Zhang, H. Peng, W. Wang and T. Liu, *Compos. Sci. Technol.*, 2011, **71**, 791-796.

**Table 1** TGA analysis results of PP/AMO–DDS– and stearic–LDH nanoconposites.

Sample	$T_{0.1}/^{\circ}\text{C}$ <sup>a</sup>	$\Delta T_{0.1}/^{\circ}\text{C}$ <sup>c</sup>	$T_{0.5}/^{\circ}\text{C}$ <sup>b</sup>	$\Delta T_{0.5}/^{\circ}\text{C}$ <sup>c</sup>
neat PP	280	NA	331	NA
PP/5 wt% (DDS)	277	-3	360	29
PP/10 wt% (DDS)	274	-6	368	37
PP/15 wt% (DDS)	260	-20	354	23
PP/20 wt% (DDS)	233	-47	343	12
PP/5 wt% (stearic)	288	8	367	36
PP/10 wt% (stearic)	335	55	398	67
PP/15 wt% (stearic)	325	45	406	75
PP/20 wt% (stearic)	326	46	411	80

<sup>a</sup> $T_{0.1}$  = temperature at 10% weight loss; <sup>b</sup> $T_{0.5}$  = temperature at 50% weight loss; <sup>c</sup> $\Delta T$  = difference between neat PP and its nanocomposites.

**Table 2** MCC analysis results of PP/AMO–DDS– and stearic–LDH nanocomposites.

Sample	PHRR <sup>c</sup> /Wg <sup>-1</sup>	Reduction /%	THR <sup>b</sup> /kJg <sup>-1</sup>	T <sub>max</sub> <sup>d</sup> /°C	HRC <sup>a</sup> /Jg <sup>-1</sup> K <sup>-1</sup>
neat PP	1640	NA	47.4	478.6	1170
PP/5 wt% (DDS)	1040	37	37.2	476.8	1020
PP/10 wt% (DDS)	861	48	33.5	475.2	1073
PP/15 wt% (DDS)	755	54	27.0	478.3	739
PP/20 wt% (DDS)	696	58	28.8	473.1	717
PP/5 wt% (stearic)	1114	33	42.6	460.8	1059
PP/10 wt% (stearic)	808	51	40.0	469.7	782
PP/15 wt% (stearic)	752	54	38.7	472.4	722
PP/20 wt% (stearic)	644	61	30.7	464	833

<sup>a</sup>HRC = heat release capacity; <sup>b</sup>THR = total heat release; <sup>c</sup>PHRR = peak heat release rate; <sup>d</sup>T<sub>max</sub> = temperature at maximum pyrolysis rate.

**Table 3** TGA analysis results of PP/AMO–stearic–LDH nanocomposites.



Sample	T <sub>0.1</sub> /°C	ΔT <sub>0.1</sub> /°C	T <sub>0.5</sub> /°C	ΔT <sub>0.5</sub> /°C
neat PP	280	NA	331	NA
PP/15 wt% (stearic/5 h)	330	50	386	57
PP/20 wt% (stearic/5 h)	324	44	387	58
PP/15 wt% (stearic/10 h)	325	45	406	75
PP/20 wt% (stearic/10 h)	326	46	411	80
PP/15 wt% (stearic/24 h)	325	45	390	59
PP/20 wt% (stearic/24 h)	338	58	396	65
PP/15 wt% (stearic/72 h)	307	27	382	51
PP/20 wt% (stearic/72 h)	299	19	390	59

**Table 4** MCC analysis results of PP/AMO–stearic–LDH nanocomposites.

Sample	PHRR /Wg <sup>-1</sup>	Reduction /%	THR /kJg <sup>-1</sup>	T <sub>max</sub> /°C	HRC /Jg <sup>-1</sup> K <sup>-1</sup>
neat PP	1640	NA	47.4	478.6	1170
PP/15 wt% (stearic/5 h)	577	65	31.9	439.8	982
PP/20 wt% (stearic/5 h)	553	66	31.5	451	524
PP/15 wt% (stearic/10 h)	752	54	38.7	472.4	722
PP/20 wt% (stearic/10 h)	644	61	30.7	464	833
PP/15 wt% (stearic/24 h)	499	70	29.5	457.7	995
PP/20 wt% (stearic/24 h)	496	70	31.1	473.4	487
PP/15 wt% (stearic/72 h)	795	52	36.3	472.7	768
PP/20 wt% (stearic/72 h)	673	59	34.9	471.7	900

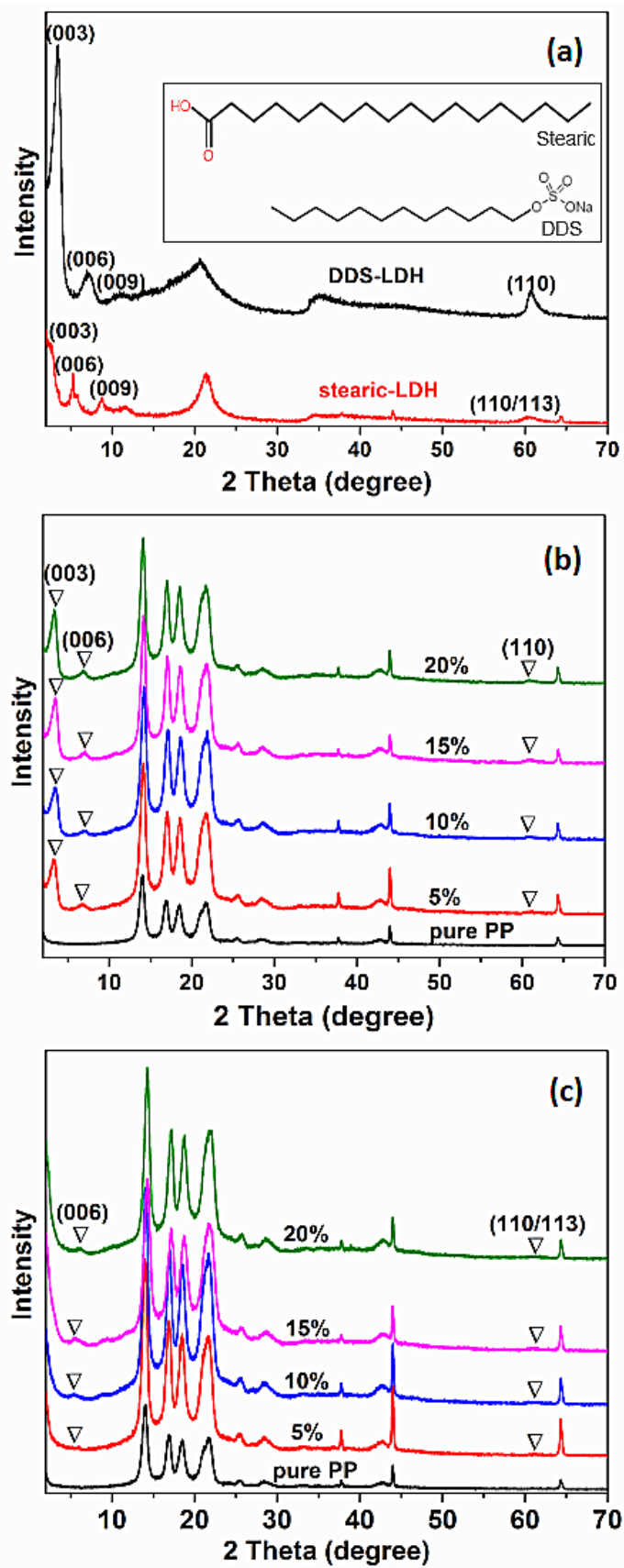


**Fig. 1** XRD patterns of (a) AMO-DDS and stearic-LDHs, (b) PP/AMO-DDS-LDH nanocomposites and (c) PP/AMO-stearic-LDH nanocomposites.

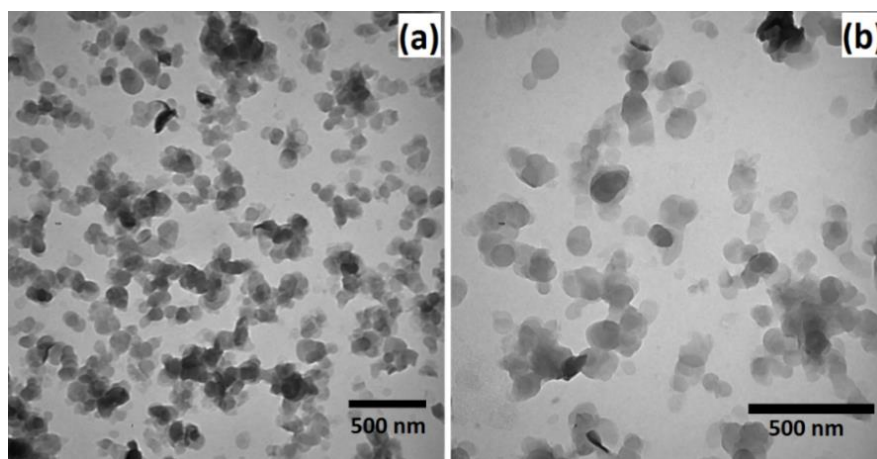


**Fig. 2** TEM images of (a) AMO-DDS-LDHs and (b) AMO-stearic-LDHs.

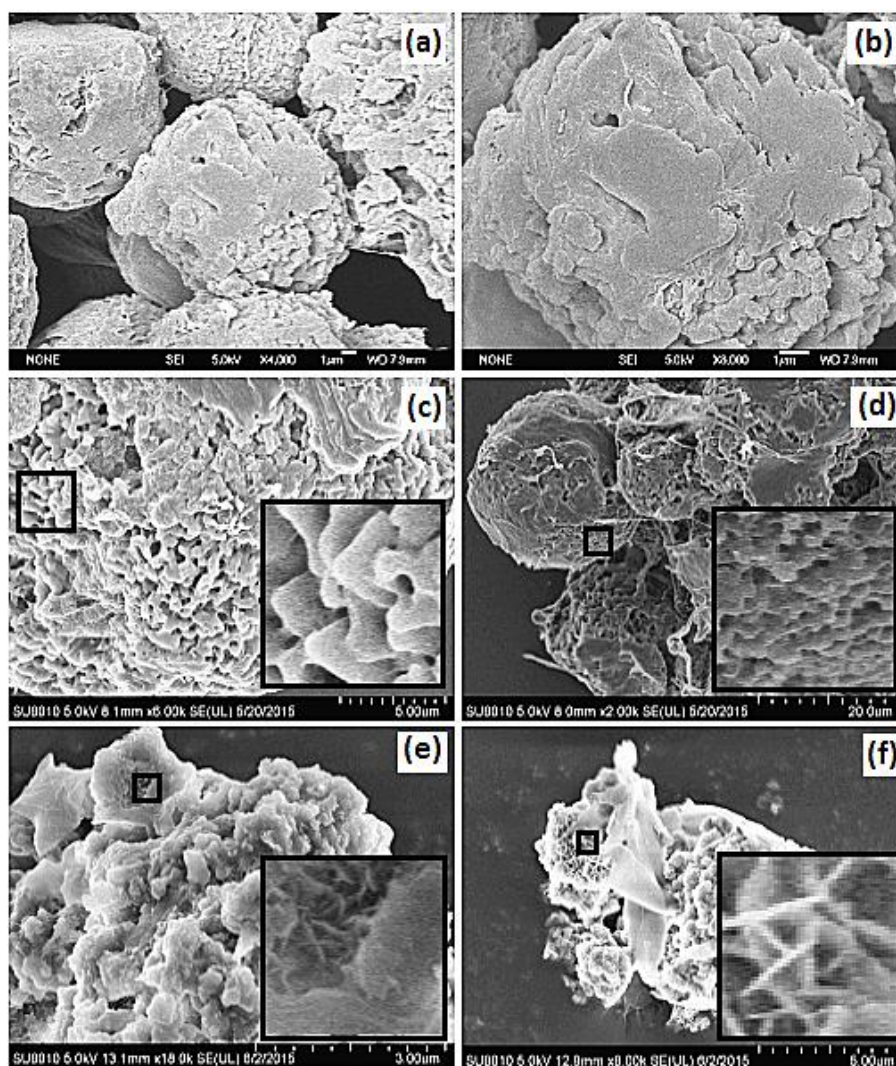


**Fig. 3** SEM images of (a–b) neat PP, PP/AMO–DDS–LDH nanocomposites with a LDH loading of (c) 5 wt%, (d) 20 wt%, and PP/AMO–stearic–LDH nanocomposites with a LDH loading of (e) 5 wt%, (f) 20 wt%.

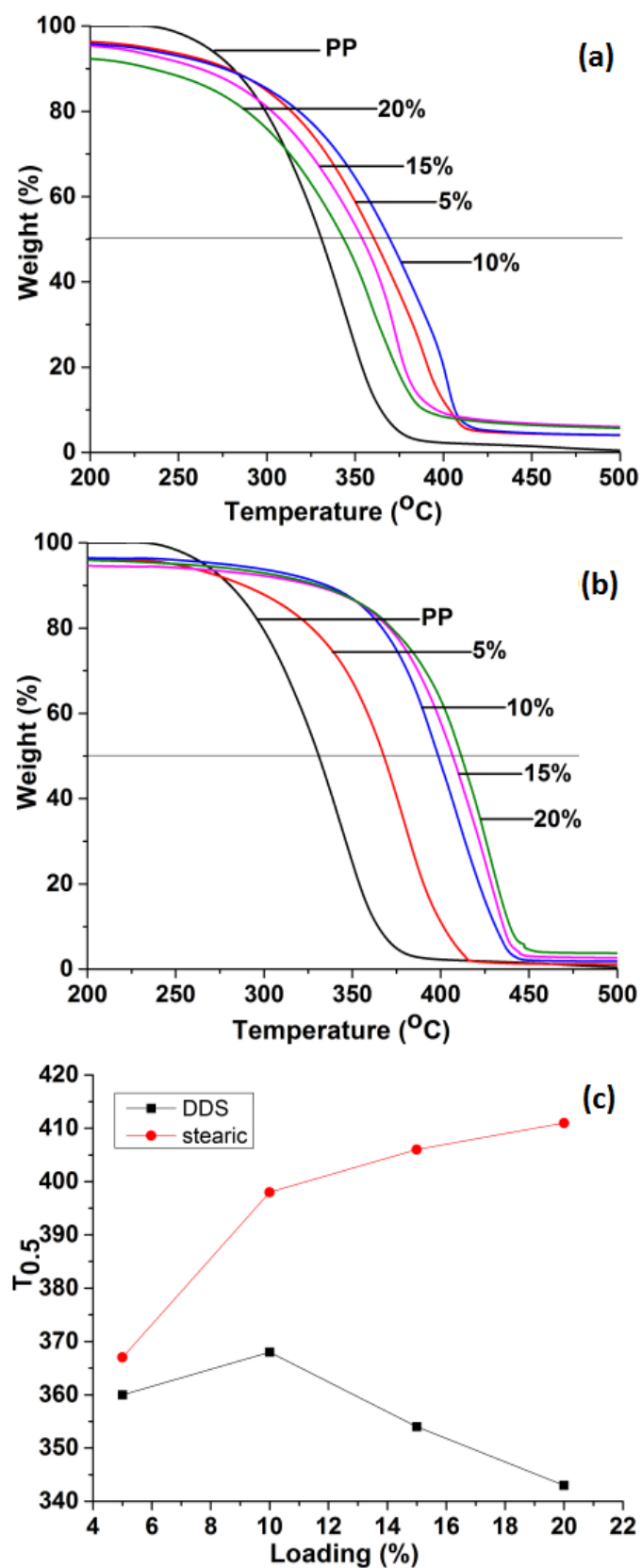


**Fig. 4** TGA analysis of (a) PP/AMO-DDS-LDH nanocomposites, (b) PP/AMO-stearic-LDH nanocomposites and (c) graph of  $T_{0.5}$  vs LDHs loading.

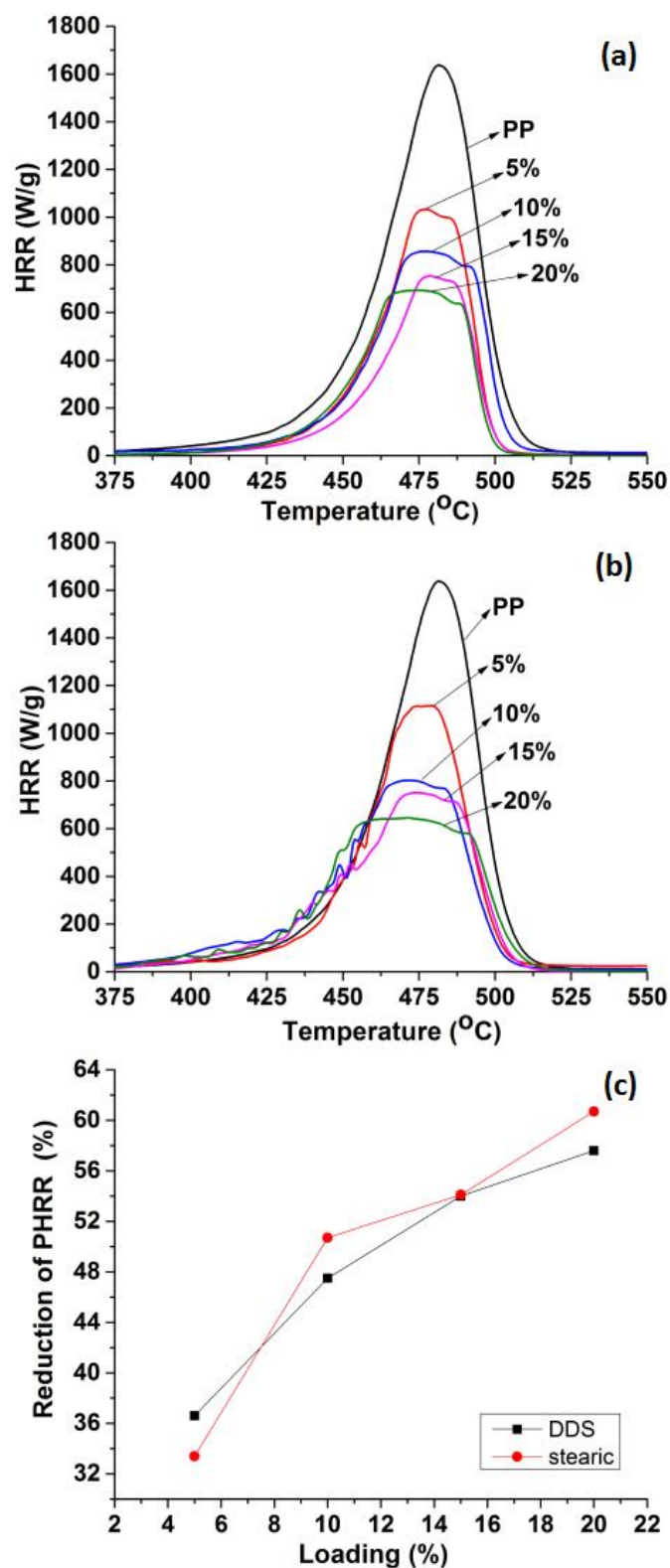


**Fig. 5** MCC analysis of (a) PP/AMO-DDS-LDH nanocomposites, (b) PP/AMO-stearic-LDH nanocomposites and (c) PHRR reduction of nanocomposites vs LDHs loading.

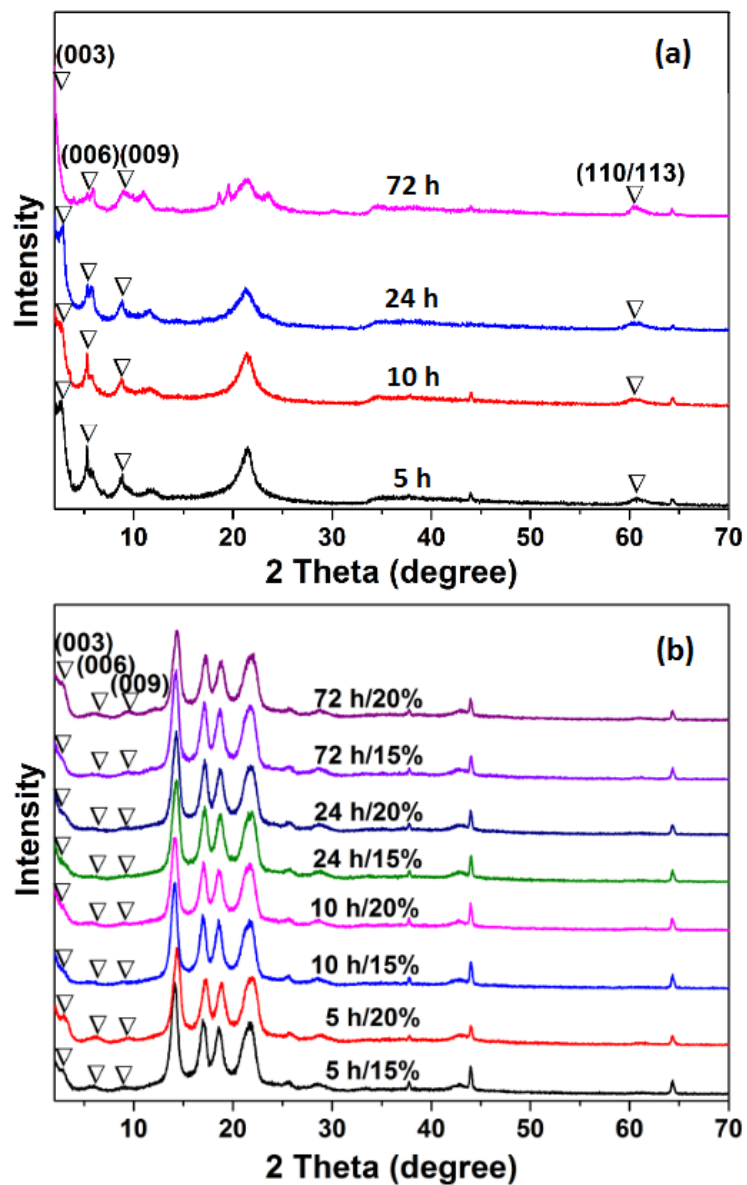


**Fig. 6** XRD patterns of (a) AMO–stearic–LDHs under different solvothermal time and (b) its nanocomposites with different LDHs loadings.



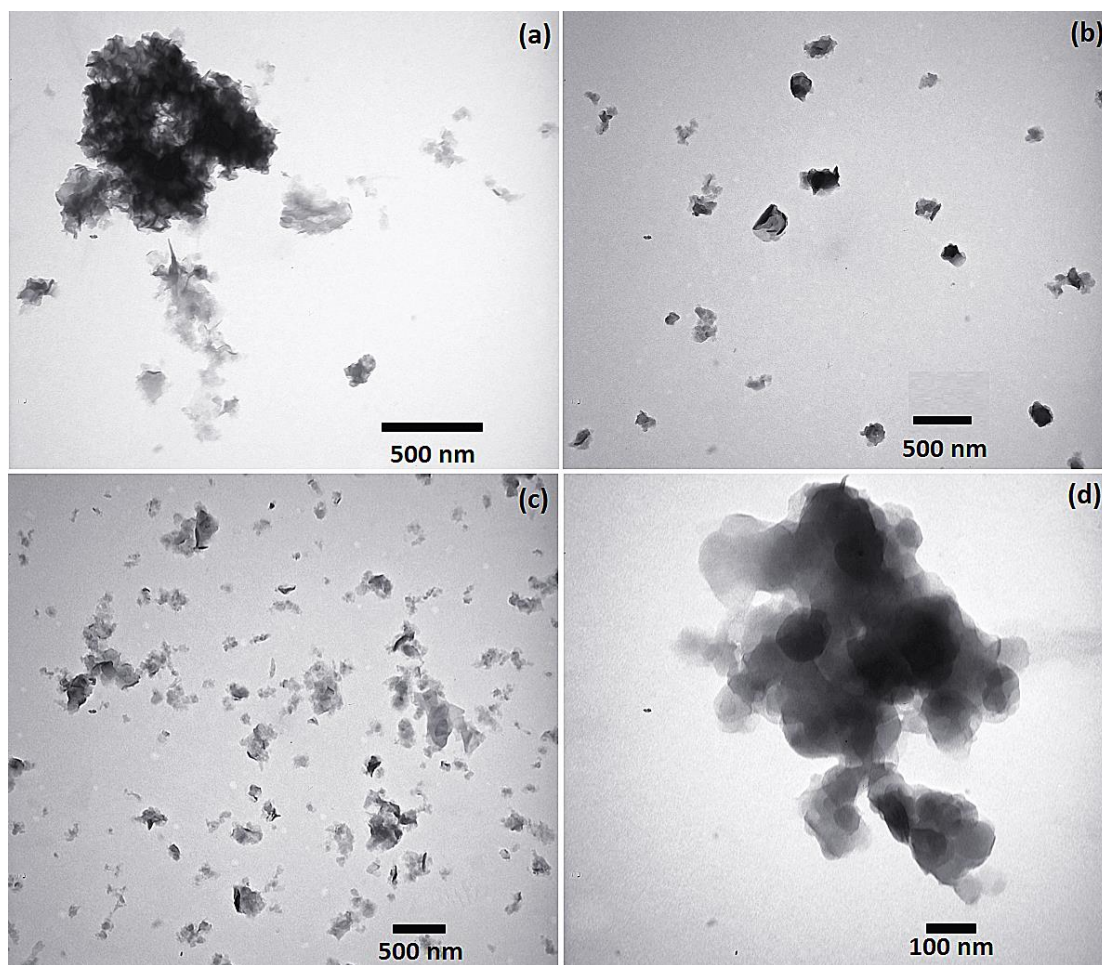


**Fig. 7** TEM images of AMO-stearic-LDHs under different solvothermal time including (a) 5, (b) 10, (c) 24 and (d) 72 h.

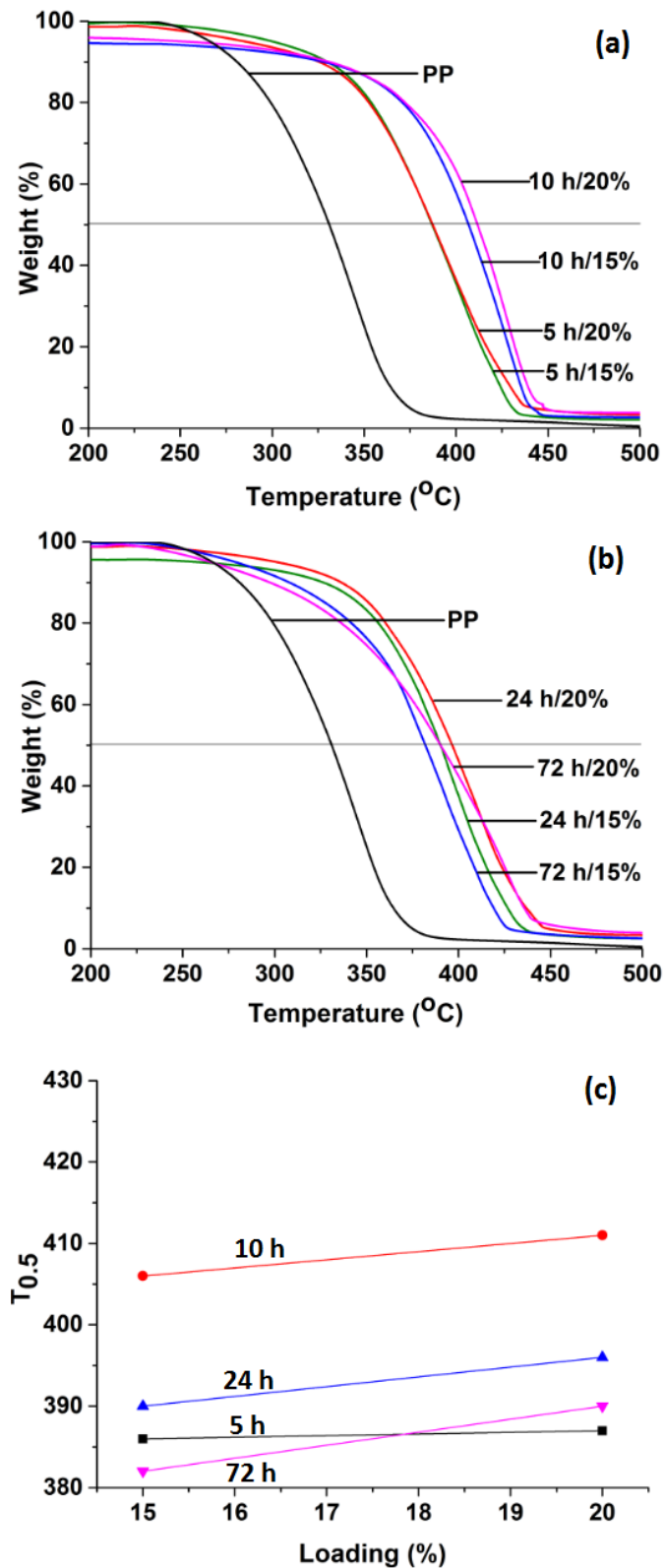


**Fig. 8** TGA analysis of (a) PP/AMO-stearic-LDH (5, 10 h) nanocomposites with different loadings, (b) PP/AMO-stearic-LDH (24, 72 h) nanocomposites with different loadings and (c) graph of  $T_{0.5}$  vs LDHs loading.

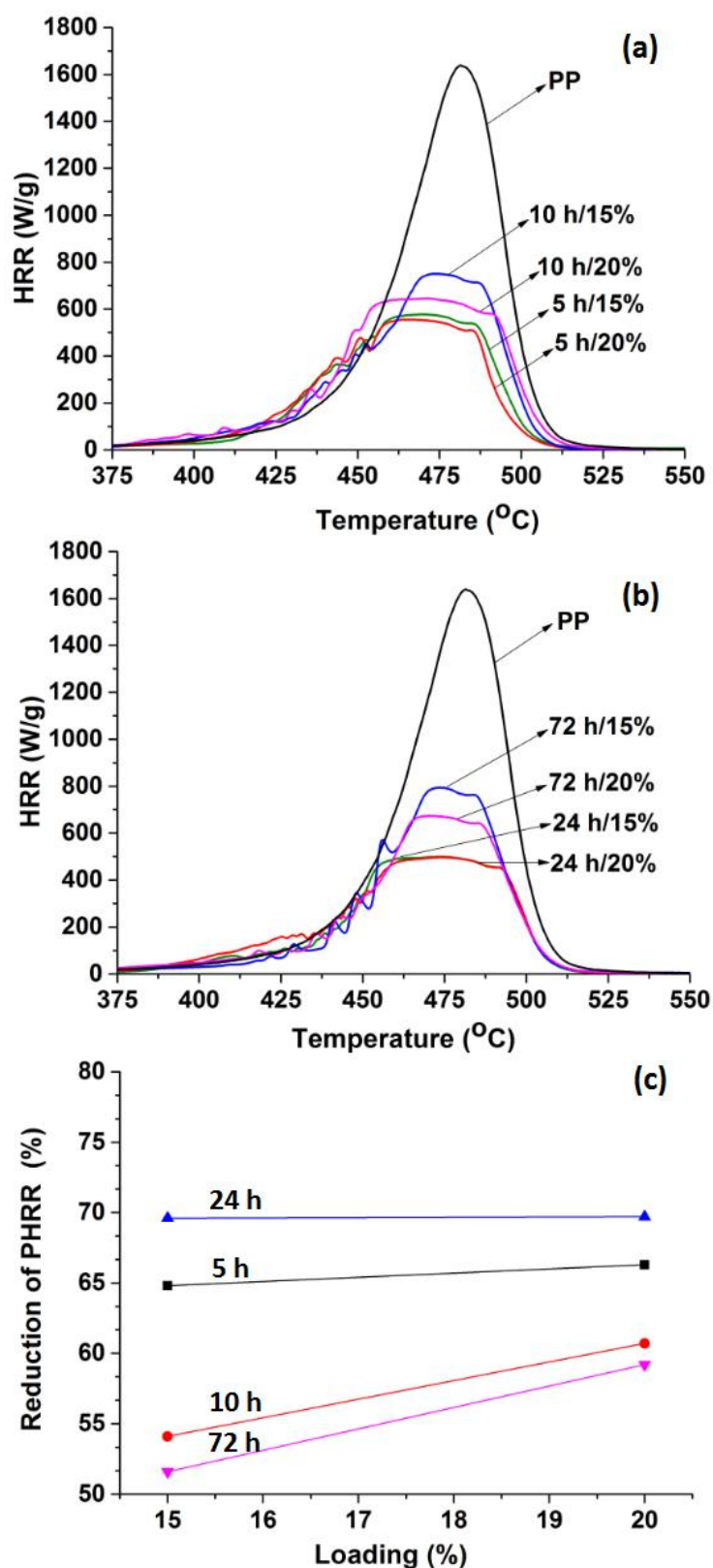


**Fig. 9** MCC analysis of (a) PP/AMO-stearic-LDH (5, 10 h) nanocomposites with different loadings, (b) PP/AMO-stearic-LDH (24, 72 h) nanocomposites with different loadings and (c) graph of PHRR reduction vs LDHs loading.